MAX-PLANCK-INSTITUT FÜR PLASMAPHYSIK

GARCHING BEI MÜNCHEN

Expression for the Thermal H-Mode Energy Confinement Time under ELM-free Conditions

F. Ryter, O. Gruber, O. J.W.F. Kardaun, H.-P. Menzler, F. Wagner
and the ASDEX and NI Teams,

D. P. Schissel,* J. C. DeBoo*, and the DIII-D Team*,

S. M. Kaye°, and the PBX-M Team°

IPP 4/257 July 1992

* General Atomics, San Diego, California, USA

° Princeton Plasma Physics Laboratory, NJ, USA

EXPRESSION FOR THE THERMAL H–MODE ENERGY CONFINEMENT TIME UNDER ELM–FREE CONDITIONS

F. Ryter, O. Gruber, O.J.W.F. Kardaun, H.-P. Menzler,
F. Wagner, and the ASDEX and NI Teams,

Max-Planck-Institut für Plasmaphysik, Euratom-Association,
Garching bei Muenchen, Germany

D.P. Schissel, J.C. DeBoo, and the DIII–D Team,

General Atomics
San Diego, California, USA

S.M. Kaye and the PBX–M Team

Princeton Plasma Physics Laboratory
Princeton, New Jersey, USA

ABSTRACT. *The design of future tokamaks, which are supposed to reach ignition with the H–mode, requires a reliable scaling expression for the H–mode energy confinement time. In the present work, an H–mode scaling expression for the thermal plasma energy confinement time has been developed by combining data from four existing divertor tokamaks, ASDEX, DIII–D, JET and PBX–M. The plasma conditions, which were as similar as possible to ensure a coherent set of data, were ELM–free deuterium discharges heated by deuterium neutral beam injection. By combining four tokamaks, the parametric dependence of the thermal energy confinement on the main plasma parameters, including the three main geometrical variables, was determined. Assuming a power law dependence, one obtains for the H–mode in deuterium by linear regression:*

$$\tau_{\rm th} = 0.066\, {\rm I_p}^{1.11\pm0.04}\, {\rm P_L}^{-0.51\pm0.03}\, R^{1.75\pm0.08}\, a^{-0.30\pm0.07}\, \kappa^{0.18\pm0.09}\, {\rm B_T}^{0.15\pm0.07}.$$

The density dependence is found to be close to zero. This expression is compared with the existing scaling relations and the differences are analyzed. Predictions for ITER are given and discussed with particular emphasis on the uncertainties. Finally, it is shown that taking the improved H–mode confinement into account by means of a simple multiplier in front of an L–mode confinement scaling expression is valid for ITER, but is not necessarily universally valid.

1. INTRODUCTION

One of the primary goals of controlled thermonuclear tokamak research is to maximize the energy confinement time τ_E during auxiliary heating and thereby ease the requirements for creating an ignited plasma. The most promising energy confinement regime is the H–mode, which was discovered in 1982 in ASDEX [1], and has since been confirmed and intensively studied under various conditions in many machines [2–12]. Knowing the parametric dependences of H–mode confinement is of crucial importance for designing next–generation devices such as ITER. Until recently, these designs were based on energy confinement time predictions derived from L–mode scaling expressions where the H–mode confinement was taken into account by a numerical enhancement factor, f_H, above the L–mode value. Among the numerous L–mode scaling relations, the ITER89–P scaling expression [13] was developed for the ITER confinement study and is now considered as the L–mode reference for plasma performance comparisons and predictions. For the present ITER design to reach ignition, f_H must be approximately 2. This condition is met experimentally for the H–mode in existing tokamaks. It is not clear, however, that the H–mode confinement time has parametric dependences similar to as ITER89–P. While the dependence on the heating power, plasma current, magnetic field and density can be studied for each machine individually, the variation of the confinement time with machine size must be studied by comparing the results of differently sized tokamaks. This was the aim of earlier analyses such as the ASDEX/JET study [14], the DIII–D/JET work [15] and the ITER H–mode database study [16,17]. In [14], the confinement time was investigated with attention to the low and high q regimes. In [15], the authors analyzed the thermal energy confinement time for a cautiously chosen limited set of ELM–free H–mode discharges obtained under similar operating conditions. As only two machines were compared, it was possible to determine the H–mode confinement dependence on just one of the geometrical parameters. For the ITER H–mode database [17], global energy confinement data from six tokamaks were assembled and the confinement times were analyzed statistically, giving the dependence on all parameters included. The approach of selecting a reduced number of well–analyzed and comparable discharges, as in [15], has the advantage of reducing the uncertainties for the scaling expression. Furthermore, the thermal energy confinement time value is particularly relevant to ITER. The work presented here is an extension of the previous DIII–D/JET study. ASDEX and PBX–M data from discharges with

similar experimental conditions were added to the existing DIII–D/JET database of reference [15]. This allowed the thermal energy confinement dependence on the three main geometrical parameters, major radius, R, minor radius, a, and elongation, κ, to be studied by regression analysis. The paper is organized as follows: Section 2 describes the experimental conditions and parameter range of the database; Section 3 describes the confinement analysis and the results of the regression analysis, which are compared with other scaling expressions; Section 4 is dedicated to discussion of the results and their implications for ITER.

2. EXPERIMENTAL CONDITIONS

The database contains 52 discharges from ASDEX, 20 from DIII–D, 75 from JET and 9 from PBX–M. The JET and DIII–D data are those used in [15] and subsequently included in the ITER H–mode database, the PBX–M discharges were selected from the ITER H–mode database and fully re–analyzed. The ASDEX data were specifically chosen for the present work and introduced into the updated ITER database in December 1991. The experimental conditions for the four machines were as similar as possible. They are described in detail for DIII–D and JET in [15] and only the main features are recalled here.

Obtaining sets of comparable discharges for the four machines was made possible essentially by selecting only ELM–free H–modes to avoid uncertainties with energy losses due to ELMs (Edge Localized Modes). Moreover, only deuterium discharges heated with deuterium neutral beams were selected, in order to avoid the uncertainties associated with isotope effects. As a consequence, the atomic mass dependence will not appear in the results. For ASDEX, DIII–D and JET, the plasma configuration was single-null, the ion drift direction pointing towards the X–point, which gives the lowest power threshold allowing exploration of a wide parametric window. For PBX–M, a double-null configuration was used. The plasma shapes, represented in Fig. 1, were elongated for DIII–D, JET and PBX–M with $\kappa = 1.6$–1.8, whereas ASDEX was basically circular with $\kappa = 1$. The effect of indentation and triangularity on confinement for PBX–M cannot be taken into account, but, as shown in Fig. 1, these geometrical effects only influence the outer flux surfaces in these discharges and are not expected to modify the global confinement time to an appreciable extent. The divertor geometries were different: ASDEX had a so-called closed divertor geometry, whereas DIII–D, JET

and PBX–M had open divertor geometries. The possible influence of this effect will be discussed in Section 3.

The ranges of the main parameters are indicated in Fig. 2 and Table I.

Table I

Parameter Range

	ASDEX	DIII–D	JET	PBX–M
Number of discharges	52	20	75	9
R [m]	1.68	1.68	2.85	1.60
a [m]	0.39	0.61	1.09	0.26
κ	1.0	1.8	1.8	1.6
R/a	4.3	2.7	2.6	6.2
I_p [MA]	0.22-0.46	0.6-2.0	2.0-4.5	0.3-0.34
B_T [T]	1.2-2.8	2.1	2.2-2.5	1.4
q_{95}	2.5-4.6	3.3-9.7	3.3-6.5	4.3
n_e [10^{19}/ m^{-3}]	3.2-4.2	3-9	2-5	2.8- 5.2
P_{beam} [MW]	1.2-2.7	1.8-10	5-10	2-6
NBI geometry	tangential	quasi-perp.	quasi-perp.	perp. and tangential

Worth noting in Table I is the wide aspect ratio ($A = R/a$) range. For DIII–D [18] and possibly JET [19] the confinement was seen to degrade at low q, probably due to the increasing sawtooth activity and, so, as in the DIII–D/JET work, only discharges with $q_{95} \gtrsim 3$ are included. This limitation was not applied to the ASDEX or PBX–M data, which do not show confinement degradation at low q. As a matter of fact, the sawtooth activity in ASDEX ELM–free H–modes is reduced in relation to an L–mode with similar parameters. The ASDEX discharges with boronization were chosen because they were obtained over wide I_p, B_T and power ranges and had reduced radiation losses. The effect of boronization on confinement time, in ASDEX, was shown in [20] not to be measurable.

An example of the temporal evolution of a typical discharge used for this study is given in Fig. 3 for ASDEX. The PBX–M time traces look very similar. Examples for DIII–D and JET are given in the DIII–D/JET work [15]. The L–H transition is indicated by the D_α light reduction in the divertor. At the same time, due to the improved confinement, the stored plasma energy strongly increased and reached a maximum determined either by radiation or by the occurrence of ELMs as in Fig. 3. As already adopted in the DIII–D/JET work, the confinement analysis was not performed at the time when the total plasma energy (W) was at a maximum but at the time when the slope (dW/dt) of W was about 30% of the total heating power. The reasons for this choice are justified and discussed in Section 3. After the L–H transition, due to the strongly improved particle confinement, the density rose in an uncontrolled fashion throughout the ELM–free phase even with no external gas input. For this study, the density was therefore not a chosen value but was determined by the time of the analysis. The radiation power also increased during the ELM–free phase but the fractional radiated power was at most 40% of the input power at the time of the analysis.

3. CONFINEMENT ANALYSIS AND SCALING STUDY

3.1. Confinement Time Analysis

To be consistent with the philosophy of performing the study under similar conditions for each device, we chose to analyze the thermal confinement time, τ_{th}. The confinement time, τ_E, derived from the total stored energy is influenced by the fast beam ion population, which differs from machine to machine, so that a study of τ_E would require taking additional parameters into account to characterize the fast ions. As usual, the thermal confinement time is calculated from

$$\tau_{th} = W_{th}/(P_T - dW/dt) \quad ,$$

where W_{th} is the thermal plasma energy and P_T is the sum of the absorbed beam power (P_{abs}) and residual Ohmic power. The absorbed beam power, in this case, is the beam power going into the torus diminished by shine–through, charge exchange and orbit losses. W_{th} is given either by the kinetic energy from T_e, T_i, Z_{eff} and n_e profiles, or by the stored energy from magnetic measurements less the contribution of the fast beam ions. For DIII–D, except for the 2 MA discharges, W_{th} was given

by the kinetic data. For ASDEX, JET, PBX–M and DIII–D at 2 MA, the second method was used and the fast ion contribution was calculated. For DIII–D at 2 MA, the plasma energy was taken from the equilibrium beta and the contribution of the fast ions was estimated from the formula $W_{fast} \sim \langle T_e \rangle^{3/2} P_{abs}/n_e$, where $\langle T_e \rangle$ is the volume–averaged electron temperature and P_{abs} is the absorbed beam power. This formula was normalized to transport calculations. For JET, the plasma energy was taken from the diamagnetic loop and the fast beam ions were calculated by a Fokker–Planck code including experimental profiles to determine the birth place of the ions. For ASDEX, the plasma energy was given by the diamagnetic loop and the stored fast ion energy was calculated from $W_{fast} = 0.024\ T_e(0)^{0.85}\ P_{abs}/n_e^{0.8}$ [MJ, keV, MW, 10^{19}, m^{-3}]. This formula was determined by TRANSP calculations performed on a subset of the ASDEX dataset. For PBX–M, the plasma energy is given by beta equilibrium and, similarly to ASDEX, a method based on TRANSP calculations was applied to calculate the fast ion contribution. The errors in the thermal energy are estimated to be 15% for DIII–D and JET, 20% for ASDEX and 25% for PBX–M.

As indicated in the previous section, the confinement analysis was performed at the time where $0.25\ P_T \lesssim dW/dt \lesssim 0.35\ P_T$. Under this condition, the radiated power was low enough so that no radiation correction to the confinement time was necessary. Moreover, because of this approach, the ASDEX discharges at low magnetic field which eventually reached the beta limit were not affected by the beta limit at the time of the analysis and therefore could be included in the database.

3.2. Regression Analysis

A combined analysis of the four datasets is greatly simplified if the power and plasma current dependences are similar for each device. This condition is fulfilled for ASDEX, DIII–D and JET, as is shown by the individual regression analyses:

ASDEX: $\tau_{th} = 0.266\, I_p^{1.20\pm0.22}\, P_L^{-0.7\pm0.23}\, B_t^{0.15\pm0.25}$,

DIII–D: $\tau_{th} = 0.251\, I_p^{0.93\pm0.17}\, P_L^{-0.49\pm0.10}$,

JET: $\tau_{th} = 0.473\, I_p^{1.04\pm0.08}\, P_L^{-0.44\pm0.10}$.

The units are s, MA, MW, m, T and $P_L = (P_T - dW/dt)$. The errors in the exponents are obtained by propagating the experimental uncertainties given in the previous section for each device.

The limited amount of PBX–M data suited to the present work only allowed the power dependence to be determined on the assumption that the energy confinement time is proportional to the plasma current. The regression yields:

PBX–M: $\tau_{th} = 0.24\, I_p^{1.00}\, P_L^{-0.88\pm0.25}$ ($I_p^{1.00}$ imposed).

The magnetic field dependence could not be individually determined for DIII–D, JET and PBX–M because of the limited B_T range in the data. This point is discussed later in this section. As shown by Fig. 2 and Table I, the uncontrolled density rise during the ELM-free phase leads to very different density ranges from device to device. Moreover, a strong correlation (90%) of density with plasma current is observed in DIII–D and to a lesser extent in JET (70%), as well as a correlation (60%) between density and power in JET and PBX–M. For these reasons, the density dependence was set to zero in the expressions given above. However, the present data give an indication that the density dependence is weak if we assume an $I_p^{1.00}$ dependence, yielding for DIII–D alone $\tau_{th}/I_p \sim P_L^{-0.49\pm08}\, n_e^{-0.02\pm12.0}$. Similarly, selecting JET data for $P_L = 6.6\pm0.7$ MW, which leaves density and current ranges intact, gives $\tau_{th}/I_p \sim n_e^{0.13\pm15.0}$. Furthermore, the fact that for a narrow density range (see Table I), ASDEX shows I_p and P_L dependences similar to those of DIII–D and JET also suggests a weak density dependence.

The combined database shows a 60% correlation between n_e and R, essentially due to DIII–D data. This would influence the result of the regression. Following the above procedure, one can confirme the weak density dependence by combining ASDEX, DIII–D and PBX–M. These devices have a very similar R value which permits one to look directly at the n_e dependence for this value of R. The regression, performed on τ_{th}/I_p to avoid the influence of the correlation between n_e and I_p in DIII–D, gives $\tau_{th}/I_p \sim n_e^{0.02\pm0.07}$. The density dependence is therefore assumed to be zero in the remaining analysis.

The regression analysis applied to the combined database of the four tokamaks yields

$$\tau_{th} = 0.066\, I_p^{1.11\pm0.04}\, P_L^{-0.51\pm0.03}\, R^{1.75\pm0.08}\, a^{-0.30\pm0.07}\, \kappa^{0.18\pm0.09}\, B_T^{0.15\pm0.07} \quad , \qquad (1)$$

with $\chi^2 = 0.277$. The units are the same as above. Here and in all following results, the errors indicate one standard deviation based on the root mean squared error (rmse) estimated from the data. The quality of the fit is illustrated in Fig. 4, where the experimental confinement time is plotted versus the predicted confinement time from Eq. (1). The rmse of the data compared with the fitted values is 8%. The experimental errors in $\tau_{\rm th}$ indicated in Fig. 4 show that all machines are well represented by the fit within their individual uncertainties. Figure 5 gives complementary statistical information for each device compared with the fit.

Equation (1) has a plasma current and heating power dependence that is similar to that observed on individual machines, thus justifying the regression on the combined database. The strong R dependence confirms the importance of this parameter for future tokamak design, as inferred from L–mode studies, and will be discussed in Section 4. The comparatively weak dependence on a indicates that the linear dimension L introduced in the DIII–D/JET study was essentially R.

Although the a dependence is not strong, it is convenient for comparison to introduce the aspect ratio $A = R/a$ explicitly into Eq. (1):

$$\tau_{\rm th} = 0.066\, {\rm I_p}^{1.11\pm0.04}\, {\rm P_L}^{-0.51\pm0.03}\, R^{1.45\pm0.05}\, A^{0.30\pm0.07}\, \kappa^{0.18\pm0.09}\, {\rm B_T}^{0.15\pm0.07} \quad . \qquad \text{(1b)}$$

The confinement increase with aspect ratio is weaker than the L–mode scaling relations of Goldston ($A^{0.37}$) [21] or Kaye–Goldston ($A^{0.49}$) [22]. Particularly important for ITER is the positive A dependence found here, in contrast to the negative one shown by ITER89–P ($A^{-0.30}$) [13], which was used for ITER predictions. This result shows that, for confinement considerations, the aspect ratio for ITER need not be as small as possible and this could facilitate the machine design. Moreover, for a given A, the R dependence of (1b) is close to that of ITER89–P ($R^{1.5}$).

The $\rm B_T$ dependence found above for ASDEX also emerges from the combined dataset. To investigate the influence of ASDEX, which has the widest explored $\rm B_T$ range for the present data, we exclude the ASDEX data and repeat the regression. As there are only three devices, one geometrical dependence has to be imposed; $\kappa^{0.18}$,

found in Eq. 1, was chosen because of the reduced κ variation in this restricted dataset. The regression gives

$$\tau_{\rm th} \sim {\rm I_p^{1.07}\, P_L^{-0.48}}\, R^{1.79}\, a^{-0.32}\, \kappa^{0.18}\, {\rm B_t^{0.27\pm0.33}}\, (\kappa^{0.18} \text{ imposed}) \quad .$$

Due to the strong correlation (80%) between a and $\mathrm{B_T}$ in this reduced dataset, it is interesting to impose also the a dependence from (1), giving for DIII–D, JET and PBX–M

$$\tau_{\rm th} \sim {\rm I_p^{1.07}\, P_L^{-0.48}}\, R^{1.77}\, a^{-0.30}\, \kappa^{0.18}\, {\rm B_t^{0.24\pm0.29}}\, (a^{-0.30}\, \kappa^{0.18} \text{ imposed}) \quad .$$

These two results show little or no $\mathrm{B_T}$ dependence within the errors and thus agreement with ASDEX and with the combined database. A further check can be performed with the JET data used in the present work by looking for the $\mathrm{B_T}$ dependence of the confinement time normalized by an expression similar to (1) with no $\mathrm{B_T}$ dependence. This procedure gives $\mathrm{B_T^{0.27\pm0.15}}$ for JET, in agreement with the other results. This consistency of combined data with observations in single machines gives confidence in the results. However, due to the possible non-negligible impact of the $\mathrm{B_T}$ dependence on extrapolations, new data and further studies with existing tokamaks, in particular JET, seem highly desirable.

It is conceivable that one device may have a larger H–mode confinement due to, for instance, a more favorable divertor configuration or wall condition. The effects of such a possible systematic deviation are analyzed in Table II, for which the confinement was arbitrarily changed by $\pm10\%$ for only one machine, and the regression analysis was then repeated. The representation is made more convenient by using R and A as in Eq. (1b).

Table II

Factor and exponents when the confinement of one single machine is arbitrarily changed by ±10%. The last line gives the maximum deviation with respect to (1b), in % for the factor and absolutely for the exponents.

Variable	Factor	I_p	P_L	R	A	κ	B_T
Initial from (1b)	0.066	1.11	- 0.51	1.45	0.30	0.18	0.15
ASDEX +10%	0.075	1.12	-0.52	1.44	0.28	0.01	0.16
DIII–D +10%	0.086	1.10	-0.51	1.28	0.17	0.27	0.15
JET +10%	0.060	1.12	-0.51	1.63	0.32	0.17	0.14
PBX–M +10%	0.055	1.11	-0.51	1.47	0.43	0.27	0.13
ASDEX -10%	0.057	1.10	-0.51	1.47	0.32	0.39	0.15
DIII–D -10%	0.050	1.13	-0.51	1.65	0.44	0.07	0.13
JET -10%	0.075	1.10	-0.51	1.26	0.28	0.19	0.15
PBX–M -10%	0.082	1.11	-0.52	1.44	0.16	0.07	0.15
Max. deviation	25%	0.01	0.01	0.20	0.14	0.17	0.01

The I_p, B_T and P_L dependences are weakly affected by this procedure because they are varied individually in each device. The most important changes are made to the numerical factor and the geometrical parameters, in particular R, by varying the confinement time of DIII–D or JET. The circular machine, ASDEX, has the strongest influence on the κ dependence. PBX–M has the strongest effect on A. The consequences on extrapolations to ITER are discussed in Section 4.

The question of the divertor geometry was addressed in [17]. It has been suggested that ASDEX has a higher confinement time because of its closed divertor geometry. This effect was analyzed in the open and closed divertor studies in ASDEX [9], which indicated for the open divertor geometry a 30% confinement degradation of the ELMy discharges supposedly associated with the higher ELM activity. An analysis performed for ELM-free discharges of ASDEX [20] shows that the confinement time for the open

geometry is only 15% to 20% lower than that of the closed geometry. From these observations and from Table II, we infer that the ASDEX divertor geometry is not a major source of uncertainty in the present study. Moreover, the determining feature of the divertor's effect on confinement is probably not only the geometry but also the characteristics of the plasma boundary. In this respect, large hot tokamaks with open divertor geometry and an extended boundary might be comparable to smaller machines with closed divertor geometry.

3.3 Comparison With Other Scaling Expressions

The scaling given by Eq. (1) is comparable to the ITER90H–P scaling relation for the total confinement time in ELM–free discharges [17]:

$$\tau_{\mathrm{E}} = 0.082\, A_{\mathrm{i}}^{0.5}\, \mathrm{I}_{\mathrm{p}}^{1.02}\, \mathrm{P}_{\mathrm{L}}^{-0.47}\, R^{1.6}\, \kappa^{-0.19}\, \mathrm{B}_{\mathrm{t}}^{0.15} \quad . \tag{2}$$

One recognizes similar $\mathrm{I_p}$, $\mathrm{P_L}$, R, and $\mathrm{B_T}$ dependences. In reference [17], the dependences on a and $\mathrm{n_e}$ were weak with errors larger than the exponents. The magnetic field dependence was set to 0.15, as a compromise between the weak dependence generally observed in individual scans and the strong dependence (0.49–0.96) given by the combined database. In Eq. (2), τ_{E} is obtained from the total stored plasma energy and, except for ASDEX, without correcting the input power for fast ion charge exchange and orbit losses. The beam ion contribution to the plasma energy, although different from machine to machine, is always positive but is partly compensated for by the power used in Eq. (2), except for ASDEX. Thus, ASDEX's confinement time used to determine Eq. (2) was overestimated and this might introduce the negative κ dependence, as suggested by Table II. Recall that the present ASDEX dataset was not in the database used in [17]. A more quantitative comparison with our results was performed by considering the ratio of Eq. (2) to Eq. (1):

$$\tau_{\mathrm{E}}/\tau_{\mathrm{th}} = 1.75\, \mathrm{I}_{\mathrm{p}}^{-0.09}\, \mathrm{P}_{\mathrm{L}}^{0.04}\, R^{-0.15}\, a^{0.30}\, \kappa^{-0.37}\, \mathrm{B}_{\mathrm{T}}^{0.00} \quad .$$

This ratio was calculated for the data considered in this paper, giving the following results represented by the mean value and the standard deviation for each device:

1.37 ± 0.040 for ASDEX, 1.13 ± 0.032 for DIII–D, 1.21 ± 0.030 for JET and 1.04 ± 0.010 for PBX–M. These values are in agreement with the positive contribution of the fast ion population to the plasma energy, with the already included correction for fast ion losses in ASDEX, the low fast ion losses in DIII–D and JET, and the large fast ion losses in PBX–M.

Also interesting is the comparison with the ELM–free thermal confinement time expression from [17] in its unconstrained version, which can be written as

$$\tau_{\rm th}^{\rm ITERHDB} \sim {\rm I_p}^{0.81}\, {\rm P_L}^{-0.75}\, R^{2.00}\, a^{0.31}\, \kappa^{0.61}\, {\rm B_T}^{0.60}\, {\rm n_e}^{0.39} \quad . \tag{3}$$

This expression is very different from Eq. (1), showing a comparatively small $\mathrm{I_p}$ dependence, stronger $\mathrm{B_T}$ and κ dependences, a positive a dependence and a non- negligible density dependence. To compare Eq. (3) with our database, we imposed the exponent of one variable to have the same value as in Eq. (3) and performed the regression on our database.

The clear negative a dependence and the low I_p dependence cannot be reproduced by fixing one of the other exponents. The closest result to Eq. (3) is obtained by imposing ${\rm I_p}^{0.81}$, yielding with or without $\mathrm{n_e}$ dependence

$$\tau_{\rm th} \sim {\rm I_p}^{0.81}\, {\rm P_L}^{-0.55\pm0.04}\, R^{2.10\pm0.12}\, a^{0.00\pm0.06}\, \kappa^{0.60\pm0.07}\, {\rm B_T}^{0.43\pm0.06}\, {\rm n_e}^{0.22\pm0.04} \quad ,$$

$$\tau_{\rm th} \sim {\rm I_p}^{0.81}\, {\rm P_L}^{-0.49\pm0.04}\, R^{1.62\pm0.09}\, a^{0.03\pm0.07}\, \kappa^{0.71\pm0.07}\, {\rm B_T}^{0.47\pm0.06} \quad .$$

It is worth noting that the strong dependences on κ and $\mathrm{B_T}$ found in Eq. (3) are reproduced. The fits are bad, however, as shown by the high χ^2 values of 3.074 and 3.069, respectively. The 60% correlation between R and n_e in our database causes the increase of the R dependence when the density is taken into account. Such a feature might also have played a role in Eq. (3). With our database, in which the low q_{95}

data are not included, we have no reason to believe that the I_p dependence is so low. Low q_{95} data were also excluded from the analysis yielding Eq. (3) and cannot be a reason for the difference. It was also demonstrated above that the density dependence is believed to be close to zero. There is, therefore, no clear agreement between Eq. (3) and Eq. (1) and no satisfactory explanation for the difference. This discrepancy between two expressions for the thermal confinement time, Eq. (1) and Eq. (3), is in contradicion to the similarities shown between Eq. (1) and Eq. (2) for the global confinement time. This poses the question whether global and thermal energy confinement times actually scale differently.

4. DISCUSSION FOR ITER

Before applying the results of this work to ITER, we reflect on the decisions to analyse the thermal confinement and select ELM–free discharges. These choices were dictated by the goal of assembling a consistent set of data. Moreover, although fast ions might help to obtain ignition, the thermal confinement time is the relevant parameter for a future reactor. On the other hand, the present–day ELM–free H–mode, with its uncontrolled time evolution and limited duration, is certainly not suitable for long–pulse operation. The ELM–free phase might, however, be useful to reach ignition. The necessary H–mode regime for a reactor will most probably be like the stationary ELM–controlled discharges demonstrated in DIII–D [23] and ASDEX [24]. In ASDEX, the I_p dependence for such discharges is similar to that of the ELM–free H–mode [25]. Furthermore, ASDEX studies of ELMs [26] show that the ELMs are transient energy losses which do not change the underlying energy transport in the plasma core. Therefore, it seems reasonable to assume that the time–averaged confinement time of ELM–controlled discharges needed for a reactor will be lower than the ELM–free confinement but will scale like Eq. (1). Experimentally, the confinement time in steady–state ELM–controlled discharges is 15% to 30% lower than in ELM–free discharges [25,27]. The reduction factor of 0.75 assumed in the ITER confinement studies [28], although possibly somewhat too pessimistic, will be used in the rest of this discussion.

For the present ITER design [28], I_p = 22 MA, P_{heat} = 115 MW, R = 6 m, a = 2.15 m, κ = 2, B_T = 4.85 T, Eq. (1) predicts τ_{th} = 4.74 s for pure deuterium plasmas. If the isotope effect ($A_i^{0.5}$) is arbitrarily taken into account for a D/T mixture (50%/50%), the predicted thermal H–mode confinement time becomes 5.30 s. It must be pointed out that the isotope effect is rather uncertain, in particular since JET has

not observed such a dependence. These values for the ELM–free regime should be reduced by 0.75 to take into account the necessity of having stationary conditions with ELMs in a reactor, yielding thermal confinement times of 3.56 s and 3.97 s for D and D/T operation, respectively. These values reach the required range of 3 to 4 s given in [28]. The uncertainties on the predictions for ITER estimated from Table II are given in Table III and Fig. 6.

Table III
ITER confinement time predictions in seconds from Table II for present design parameters

Regime; Gas	H*; D	H*; DT	H; D	H; DT	%
from (1)	4.74	5.30	3.56	3.97	0
ASDEX +10%	4.66	5.21	3.50	3.91	-2
DIII–D +10%	4.01	4.48	3.01	3.36	-15
JET +10%	6.04	6.75	4.53	5.06	27
PBX–M +10%	4.86	5.43	3.65	4.08	3
ASDEX -10%	4.86	5.43	3.65	4.08	3
DIII–D -10%	5.66	6.33	4.25	4.75	19
JET -10%	3.61	4.04	2.71	3.03	-24
PBX–M -10%	4.58	5.12	3.44	3.84	-3

In this table, H* is for ELM-free and H is for stationary discharges ($\tau_H = 0.75\ \tau_H^*$). The last column gives the relative deviation from the initial values given by Eq. (1), assuming an isotope effect of $A_i^{0.5}$ for the D/T mixture.

Table III and Fig. 6 show that a 10% systematic error in the DIII–D or JET confinement time has a major effect on the predictions for ITER. These numbers confirm the minor role played by the ASDEX and PBX–M divertor geometries on ITER predictions. Some values for ELM–controlled cases are clearly lower than the required confinement time for ITER and this shows the potential role of the ELM–free phase to reach ignition in marginal situations. In this context, it is worth discussing the influence of errors in

the exponents of Eq. (1) and assessing the main contributions to the uncertainties of the ITER predictions. The results are summarized in Table IV, which gives the relative changes of the confinement time predicted for ITER that are induced by: a) the errors in the exponents indicated in Eq. (1); b) a 10% increase of the design parameters.

Relative changes (%) in the confinement time predicted for ITER by Eq. (1). Induced by the statistical errors in different exponents and by a 10% increase of design parameters.

	I_p	P_L	R	A	κ	B_T
exponent error	14	-15	9	8	7	15
0.10 design	11	-5	15	3	2	1

The largest sources of uncertainties linked with the errors in the exponents are I_p, P_L and B_T; the first two because of their large values for ITER and the last one because of the relatively poor determination of its dependence. However, the uncertainties on the predictions do not exceed 15%, which seems acceptable and can be improved by further studies on the presently operating tokamaks. It is interesting to note that a 10% increase of R (or I_p) compensates an eventual negative influence of heating power introduced by the statistical uncertainty on the P_L exponent. Changing the other design values has only a small effect.

As most of the ITER studies were performed with the ITER89–P scaling expression [13] multiplied by the enhancement factor $f_H = 2$ [27], it is important to check to what extent this approach was justified. The ITER89–P scaling expression is

$$\tau_E^{ITER89-P} = 0.048\, A_i^{0.5}\, I_p^{0.85}\, P^{-0.5}\, R^{1.2}\, a^{0.3}\, \kappa^{0.5}\, n_e^{0.1}\, B_T^{0.2} \quad , \tag{4}$$

and for the ITER design values it gives for deuterium $\tau_E^{ITER89-P} = 1.96$ s. The H–mode confinement time predicted by our Eq. (1) is above this value by an enhancement factor $f_H = 2.42$ for ELM–free discharges. For ELMy ones, this value would be 0.75 times

lower, i.e. $f_H = 1.8$. These predicted enhancement factors are close to the experimental values, for the ELM–free discharges of the present work, as shown in Fig. 7, and for the ELM–controlled discharges in ASDEX [9,25]. This validates, a posteriori, the use of a simple factor to estimate roughly the H–confinement time for ITER, but the final design should be based on an H–mode scaling expression.

A more general way to look at f_H is provided by the ratio of Eq. (1) to $\tau_E^{ITER89-P}$, more conveniently expressed with the aspect ratio A

$$f_H = 0.97\, I_p^{0.26}\, P_L^{-0.01}\, A^{0.55}\, a^{-0.05}\, \kappa^{-0.32}\, n_e^{0.01}\, B_T^{0.05} \quad .$$

The isotope effect cancels out if we assume it to be $A_i^{0.5}$ in both cases. This expression shows how the positive current and aspect ratio dependences compensate the negative ones. It, thus, appears that f_H is around 2 for ITER fortuitously or, more probably, because of the analogy of the device with the existing divertor tokamaks. The positive aspect ratio dependence could be used to increase f_H and therefore the margin for reaching ignition.

The negative influence of the minor radius on the confinement time shown by Eq. (1) should not lead us to forget that this parameter must be large to achieve high plasma currents and high heating powers. In fact, if we consider rather the averaged current and power densities, $j = I_p/\pi a^2 \kappa$ and $p = P_L/2\pi^2 a^2 \kappa R$ respectively, Eq. (1) becomes

$$\tau_{th} \sim j^{1.11}\, p^{-0.51}\, A^{1.24}\, a^{2.14}\, \kappa^{0.78} \quad .$$

The maximum current density, limited by the magnetic field and low–q MHD instabilities, does not vary much from machine to machine; from 1 MA m^{-2} in ASDEX to 0.75 MA m^{-2} in ITER. Due to the rapidly increasing plasma volume with machine size, the power density decreases with increasing size (from 0.5 MW m^{-3} in ASDEX to 0.1 MW m^{-3} in ITER), which moderates the confinement degradation with power. The aspect ratio and elongation are close to 3 and 2, respectively, for future devices.

Therefore, this expression indicates that H–mode confinement increases more strongly than a^2 at constant aspect ratio.

SUMMARY

An H–mode database including ASDEX, DIII–D, JET and PBX–M data from ELM–free discharges was assembled. The selection and analysis of the data were performed with the aim of having conditions which are as comparable as possible for the four machines to reduce the uncertainties. The scaling relation for the thermal energy confinement time was determined and has features comparable to the H–mode ITER90H–P scaling for the global energy confinement time. The confinement time scales quasi–linearly with the plasma current and degrades with the square root of the heating power. The major radius plays the dominant role among the geometrical variables. The other parameters, minor radius, elongation and density, show weak dependences. The positive influence of the aspect ratio on confinement might relax the requirements on the ITER design. The magnetic field dependence is in agreement with observations in single scans and this gives confidence in the results. The uncertainty in the predicted ITER confinement time due to the errors in the exponents given by the regression analysis is dominated by I_p, B_T, P_L and R; I_p and P_L because of the large design values, B_T and R because of the relatively large errors in the exponents. Consequently, further studies of the magnetic field dependence for existing tokamaks are needed. Concerning the improvement of the determination of R, an important contribution is expected from JT60–U. Comparisons with the ITER89–P L–mode scaling relation, for the values presently envisaged to reach ignition in ITER, give an enhancement factor of about 2, as is required by ITER. However, f_H can strongly vary, depending on the combination of the design values of the project.

ACKNOWLEDGMENTS

The authors are grateful to the boards of the laboratories who made this common work possible. We also thank the JET Team for allowing the use of the JET data. One author (F.R.) is particularly glad to thank Prof. R. Wilhelm and Dr. F. Wesner, who encouraged and supported this work. He also appreciated the generous and warm hospitality of his colleagues from DIII–D during his stay at General Atomics. The efforts of the technical and experimental teams are greatly acknowledged.

The work was sponsored by the U.S. Department of Energy under Contract No. DE–AC03–89ER51114 for DIII–D and DE–AC02–76–CHO–3073 for PBX–M. The ASDEX work was partly performed under EURATOM Mobility Contract No. 131–83–7–FUSC.

REFERENCES

[1] WAGNER, F., BECKER, G., BEHRINGER, K., *et al.*, Phys. Rev. Lett. **49** (1982) 1408.

[2] KAYE, S.M., BELL, M.G., BOL, K., J. Nucl. Mat. **121** (1984) 115.

[3] SCHISSEL, D.P., BURRELL, K.H., DeBOO, J.C., *et al.*, Nucl. Fusion **29** (1989) 185.

[4] ASDEX TEAM, Nucl. Fusion **29** (1989) 1959.

[5] SUZUKI, N., AIKAWA, A., HOSHINO, K., *et al.*, (Proc. 12th IAEA Int. Conf. on Plasma Physics and Controlled Nuclear Fusion, Nice 1988) Vol. 1 IAEA Vienna (1989) 207.

[6] BELL, R.E., ASAKURA, N., BARNABEI, S., Phys. Fluids, B2 **6** (1990) 1271.

[7] DIII–D TEAM, presented by STAMBAUGH, R.D., 13th IAEA Int. Conf. on Plasma Physics and Controlled Nuclear Fusion, Washington D.C., 1–6 October 1990, Paper IAEA-CN-53/A-1-4.

[8] The JET TEAM, presented by TANGA, A., 13th IAEA Int. Conf. on Plasma Physics and Controlled Nuclear Fusion, Washington D.C., 1–6 October 1990, Paper IAEA-CN-53/A-4-1.

[9] WAGNER, F., RYTER, F., FIELD, A.R., *et al.*, 13th IAEA Int. Conf. on Plasma Physics and Controlled Nuclear Fusion, Washington D.C., 1–6 October 1990, Paper IAEA-CN-53/A-4-2.

[10] TSUJI, S., IDE, S., SEKI, M., *et al.*, 13th IAEA Int. Conf. on Plasma Physics and Controlled Nuclear Fusion, Washington D.C., 1–6 October 1990, Paper IAEA-CN-53/E-1-4.

[11] IMAI, T., KIMURA, H., USHIGUSA, K., *et al.*, 13th IAEA Int. Conf. on Plasma Physics and Controlled Nuclear Fusion, Washington D.C., 1–6 October 1990, Paper IAEA-CN-53/E-1-3.

[12] LUCE, T.C., JAMES, R.A., FYARETDINOV, A., *et al.*, 13th IAEA Int. Conf. on Plasma Physics and Controlled Nuclear Fusion, Washington D.C., 1–6 October 1990, Paper IAEA-CN-53/E-1-2.

[13] YUSHMANOV, P.N., TKIZUKA, T., RIEDEL, K.S., *et al.*, Nucl. Fusion **30** (1990) 1990.

[14] KARDAUN, O.J.W.F., THOMSEN, K., CORDEY, J.G., *et al.*, Euro-Physics Conference Abstracts, 17th European Conf. on Controlled Fusion and Plasma Physics, **14B** Part I (1990) 110.

[15] SCHISSEL D.P., DeBOO J.C., BURRELL K.H., *et al.*, Nucl. Fus. **31** (1991) 73.

[16] CHRISTIANSEN, J.P., CORDEY, J.G., THOMSEN, K., *et al.*, 13th IAEA Int. Conf. on Plasma Physics and Controlled Nuclear Fusion, Washington D.C., 1–6 October 1990, Paper IAEA-CN-53/F- 3-19.

[17] CHRISTIANSEN, J.P., CORDEY, J.G., THOMSEN, K., *et al.*, Nucl. Fus. **32** (1992) 291.

[18] SCHISSEL, D.P., KELLMAN A.G., SNIDER R.T., *et al.*, Nucl. Fus. **32** (1992) 107.

[19] JET TEAM, presented by KEILHACKER, M., *et al.*, (Proc. 12th IAEA Int. Conf. on Plasma Physics and Controlled Nuclear Fusion, Nice 1988) Vol. 1 IAEA Vienna (1989) 159.

[20] RYTER, F., KARDAUN, O.J.W.F., KUS A., *et al.*, Euro-Physics Conference Abstracts, 19th European Conf. on Controlled Fusion and Plasma Physics, **16C** Part I (1992) 7.

[21] GOLDSTON, R.J., Plasma Phys. and Contr. Fusion **26** (1984) 87.

[22] KAYE, S.M., GOLDSTON, R.J., Nucl. Fus. **25** (1985) 65.

[23] MAHDAVI, M.A., KELLMAN, A., GOHIL, P., *et al.*, Euro-Physics Conference Abstracts, 16th European Conf. on Controlled Fusion and Plasma Physics, **13B** Part I (1989) 249.

[24] VOLLMER, O., ARATARI, R., RYTER, F., *et al.*, Euro-Physics Conference Abstracts, 17th European Conf. on Controlled Fusion and Plasma Physics, **14B** Part III (1990) 295.

[25] VOLLMER, O., RYTER, F., STEUER, K.H., *et al.*, Euro-Physics Conference Abstracts, 18th European Conf. on Controlled Fusion and Plasma Physics, **15C** Part I (1991) 385.

[26] WAGNER, F., GRUBER, O., GEHRE, O., *et al.*, Euro-Physics Conference Abstracts, 15th European Conf. on Controlled Fusion and Plasma Physics, **12B** Part I (1988) 207.

[27] SCHISSEL, D.P., OSBORN, T.H., CARLSTROM, T.M., *et al.*, Euro-Physics Conference Abstracts, 19th European Conf. on Controlled Fusion and Plasma Physics, **16C** Part I (1992) 235.

[28] POST, D.E., BORRASS, K., CALLEN, J.D., *et al.*, ITER Physics, ITER Documentation Series No. 21, International Atomic Energy Agency, Vienna, 1991.

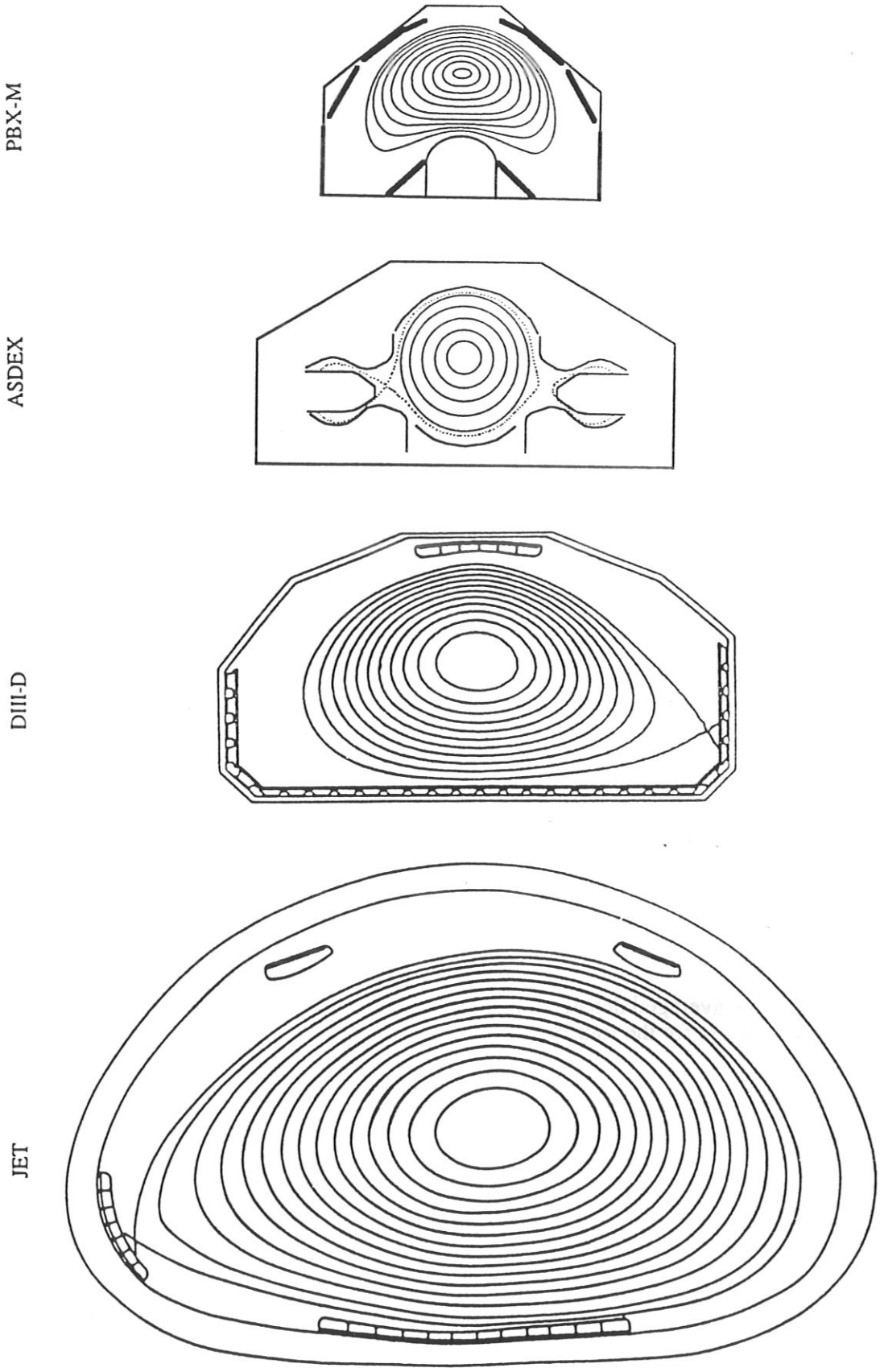

Fig. 1: Plasma shapes of the four machines. The figure is drawn to scale.

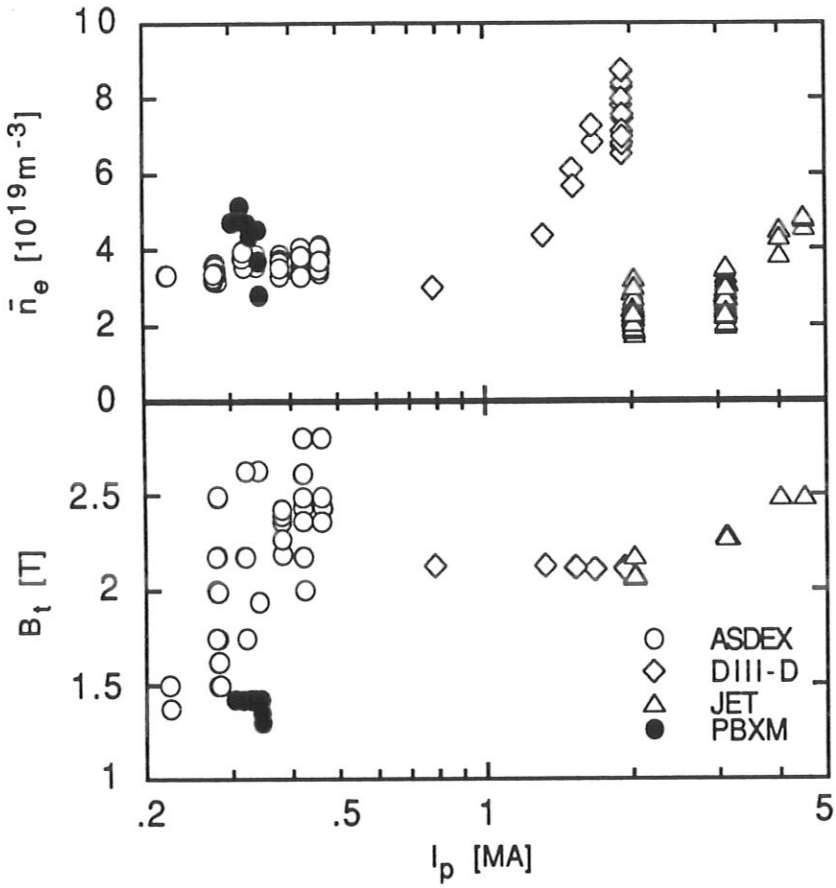

Fig. 2: Line averaged density and magnetic field values included in the database versus plasma current for the four machines.

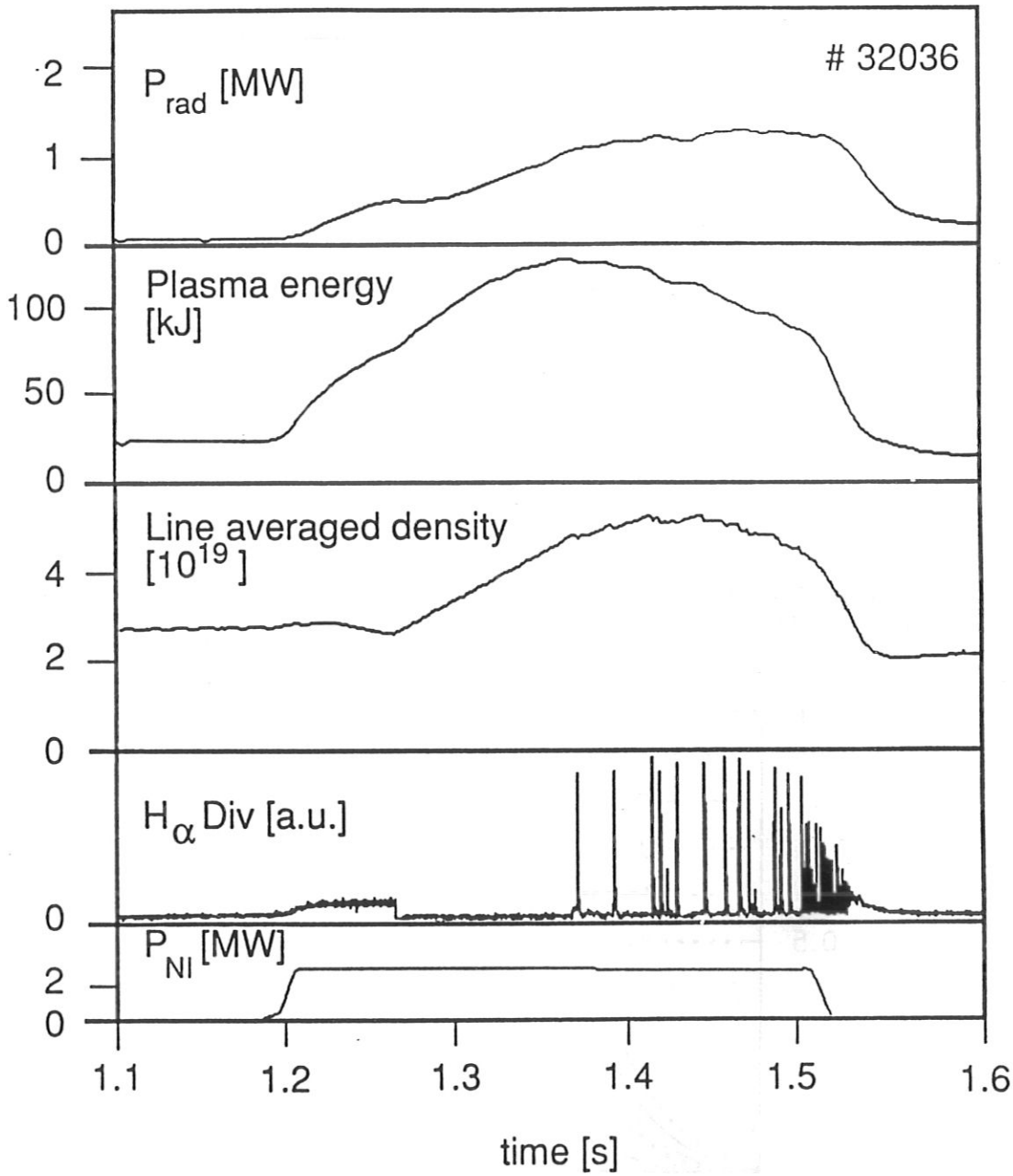

Fig. 3: Time evolution of an ELM-free ASDEX H-discharge included in the database. $I_p = 0.28$ MA, $B_t = 1.74$ T. The analysis was performed at 1.3 s.

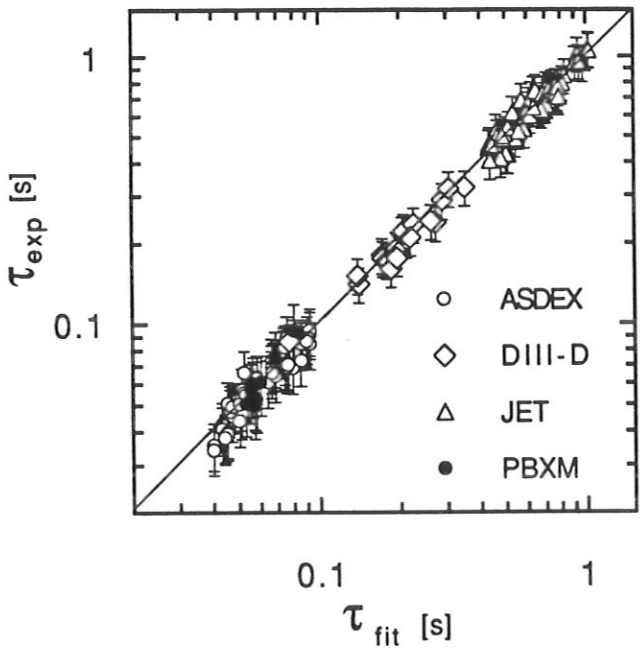

Fig. 4: Experimental thermal confinement time versus predicted thermal confinement time from Eq. (1).

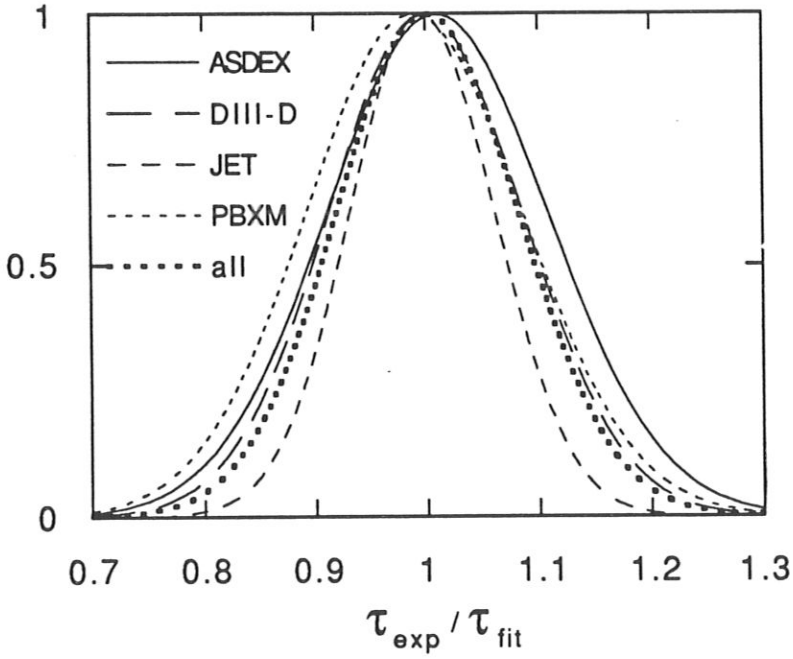

Fig. 5: Normalized Gaussian fits of τ_{exp}/τ_{fit} statistical distributions for each device and for the combined database where τ_{fit} is taken from Eq. (1).

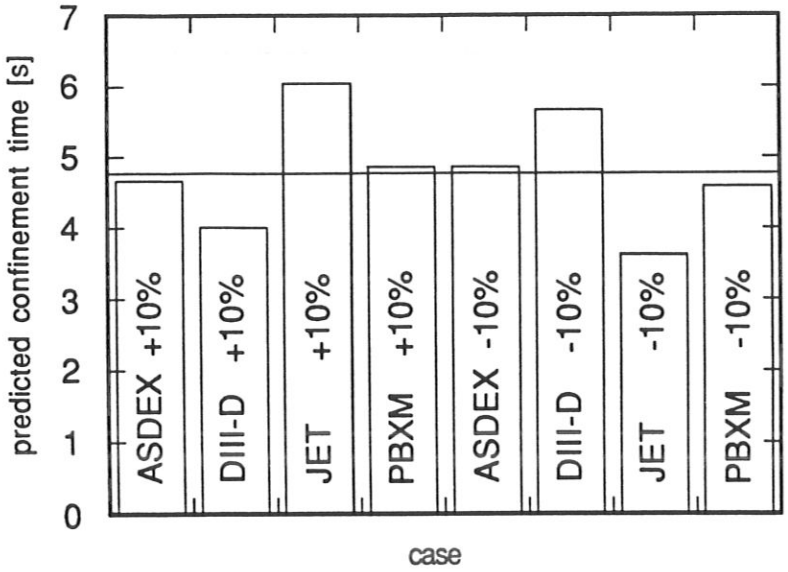

Fig. 6: Predicted thermal confinement time for ITER under different assumptions as presented in the text.

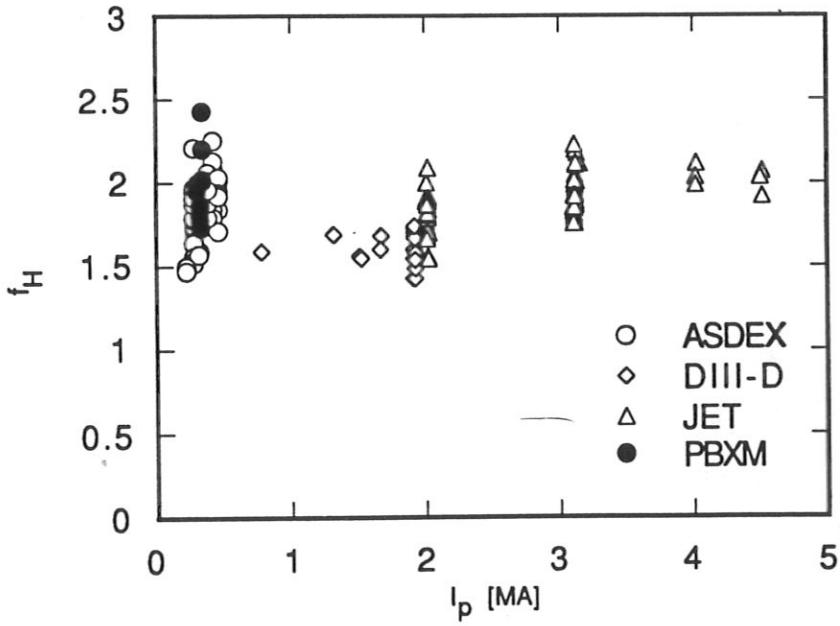

Fig. 7: Experimental enhancement factor f_H relative to $\tau_E^{ITER89-P}$ versus plasma current for the four tokamaks for the ELM-free data considered in this paper.